Acoustic Noise and Vibration Reduction of Coreless Brushless DC Motors with an Air Dynamic Bearing

Iee-Woo Yang*, Young-Seok Kim* and Sang-Uk Kim**

Abstract – This paper presents the acoustic noise and mechanical vibration reduction of a coreless brushless DC motor with an air dynamic bearing used in a digital lightening processor. The coreless brushless DC motor does not have a stator yoke or stator slot to remove the unbalanced force caused by the interaction between the stator yoke and the rotor magnet. An unbalanced force makes slotless brushless DC motors vibrate and mechanically noisy, and the attractive force between the magnet and the stator yoke increases power consumption. Also, when a coreless brushless DC motor is driven by a 120° conduction type inverter, high frequency acoustic noise occurs because of the peak components of the phase currents caused by small phase inductance and large phase resistance. In this paper, a coreless brushless DC motor with an air dynamic bearing to remove mechanical vibration and to reduce power consumption is applied to a digital lightening processor. A 180° conduction type inverter drives it to reduce high frequency acoustic noise. The applied methods are simulated and tested using a manufactured prototype motor with an air dynamic bearing. The experimental results show that a coreless brushless DC motor has characteristics of low power consumption, low mechanical vibration, and low high frequency acoustic noise.

Keywords: Coreless BLDC motor, Slotless BLDC motor, Air dynamic bearing, Stator yoke, Mechanical vibration, Acoustic noise, Power consumption, 180° conduction type inverter

1. Introduction

Recently, brushless DC motors (BLDCMs) have been placed in high value-added products including home appliances and hard disk drives because they are smaller and have higher efficiency than other types of motors. In particular, general BLDCMs with a ball bearing (BB) or fluid-dynamic bearing (FDB) have been used in small spindle motor applications. But, their friction torque causes high power consumption while cogging torque causes mechanical vibration and acoustic noise as a result of torque ripple [1][2]. Consequently, many authors have conducted research related to air dynamic bearings (ADBs) and slotless BLDCMs in order to reduce these torque components and the problem of high power consumption [3][4]. Digital lightening processors (DLPs) are used in projection TVs or when projectors are used which have a high speed color wheel which changes from white light to color light. The color wheel driven by the motor must rotate at a high and precise speed without mechanical vibration or acoustic noise in order to provide a high-resolution, high-colored image. The ADB without friction loss is appropriate for color wheel bearings which drive the motor and a slotless BLDCM without cogging torque is adequate in regards to mechanical vibration and acoustic noise. However, an ADB has a low load capacity because it uses low viscosity air as a lubricator [5], and the assembling tolerance and processing error make the air-gap difference between the magnet and the stator yoke. This occurs in the unbalanced electro-magnetic force in slotless BLDCMs. It imposes the ADB on the disturbance force and makes the DLP vibrate and noisy mechanically, and the attractive force between the magnet and the silicon steel stator yoke in the unbalanced air-gap increases power consumption. Consequently, coreless BLDCMs without a silicon steel stator yoke is appropriate for a color wheel driving motor.

A 120° or 180° conduction type inverter is used to drive coreless and slotless BLDCMs which have small phase inductance and large phase resistance. The peak component of the phase current occurs in switching or the PWM of the 120° conduction type inverter because of a low electrical time constant. Consequently, electrical acoustic noise appears in high-frequencies, and the current waveforms need to change to trapezoidal or sinusoidal waveforms.

This paper analyzes the unbalanced electro-magnetic force of slotless and coreless BLDCMs in the fabrication error and investigates the effect of the unbalanced electro-magnetic force on the ADB and DLP using finite element analysis (FEA) of the electromagnetic and mechanical fields, and proposes the reduction method of high frequency acoustic noise and mechanical vibration. In order to get the precise speed and the trapezoidal phase current waveform, a coreless BLDCM is driven by a 180° conduction type inverter applied to a space vector PWM (SVPWM), and the DC link voltage is controlled by a buck converter which is controlled by a linear quadratic regulator (LQR).

In order to prove the validity of the proposed method and

* Dept. of Electrical Engineering, Inha Univ., Korea. (iwyang@adtech21.com)
** Dept. of Electrical Information, Inha Technical College, Korea. (sanguk@inhatc.com)
Received 9 January 2009; Accepted 15 April 2009

analysis, the power consumption, mechanical vibration, and acoustic noise of a coreless and slotless BLDCM is tested using a manufactured prototype motor with an ADB. Test results prove that the proposed method reduces acoustic noise and mechanical vibration, and analysis of the appropriateness of the electromagnetic and mechanical field by FEA.

2. Air Dynamic Bearing

An ADB consists of the bearing journal and the sleeve. The bearing journal rotates in a state of eccentricity in the clearance between the journal and the sleeve because of the journal's weight and load force, etc. Eccentricity makes the bearing move in the direction of the large clearance because of air pressure difference in the clearance.

Equation (1) is the pressure equation of the ADB from the Reynolds equation [6] in a steady state. Fig. 1 shows the structure of the ADB.

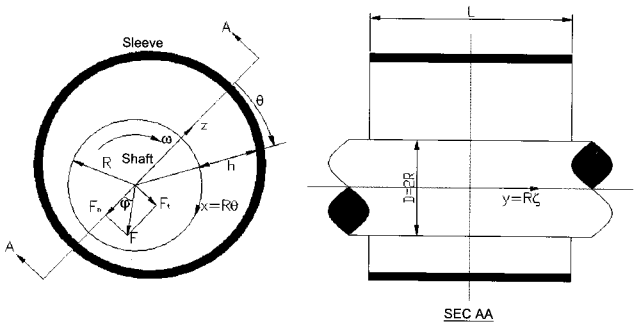

Fig. 1. Structure of the air dynamic bearing

$$\frac{\partial}{\partial\theta}(PH^3\frac{\partial P}{\partial\theta})+\frac{\partial}{\partial\varsigma}(PH^3\frac{\partial P}{\partial\varsigma})=\Lambda\frac{\partial}{\partial\theta}(PH) \tag{1}$$

where, $P=\frac{p}{p_a}$: pressure rate of the bearing for the air pressure,

p : air pressure in the bearing journal, p_a : ambient pressure

$\Lambda=\frac{6\mu\omega}{p_a}\left(\frac{R}{C_r}\right)^2$: number of bearings

$h=C_rH=C_r(1+\varepsilon\cos\theta)$: bearing clearance

μ : viscosity coefficients, R : radius of the bearing journal.

Equation (1) is linearized using the perturbation method as equation (1) is a nonlinear equation, and the pressure distribution in the bearing clearance is solved by the FEA. Also, the eccentricity directional component F_t and the perpendicular component F_n of the load capacity F are acquired by integrating to the surface by the eccentricity directional and the eccentricity perpendicular directional component of the pressure, respectively. The attitude angle θ is the angle between F_n and the load capacity F. The load capacity F of the ADB is the stress force for the disturbance.

3. Electromagnetic Field of a Coreless BLDCM

The electromagnetic field equation is deduced from the Maxwell magneto-static equation and Coulomb gauge. The governing equation of the electromagnetic field is Equation (2) which is obtained by replacing the magnetized distribution of the permanent magnet by the equivalent current density.

$$-\frac{1}{\mu_0}\nabla^2A=J+J_m \tag{2}$$

where, μ_0 : vacuum permeability,

A : magnetic vector potentials

J : stator current density by the external circuit

J_m : equivalent magnetization current density of the permanent magnet.

The Maxwell stress tensor method and Ampere's circuital law are used to find the electromagnetic torque and the unbalanced magnetic force [7]. The force density function per volume is equation (3).

$$F=\int_v f_v dv=\int_v \nabla\cdot\sigma dv=\oint_S \sigma ds \tag{3}$$

where, $f_v=\left[\nabla\times\frac{B}{\mu_0}\right]\times B=\frac{1}{\mu_0}[B(\nabla\cdot B)-B\times(\nabla\times B)]$

$\sigma_{ij}=\frac{1}{\mu_0}(B_iB_j-\frac{1}{2}B^2\delta_{ij})$,

σ : Maxwell stress tensor,

δ_{ij} : Kronecker Delta Function

Total force and torque is computed by integrating equation (3) to axis length.

4. Speed and Current Controller

This paper uses the speed control method which controls the DC link voltage to the speed reference. The buck converter controls the DC link voltage to minimize the rotating speed error between the reference speed and the real speed. It is controlled by a PI controller using an LQR that locates the optimal PI gain for disturbance and system noise. In order to make the phase current trapezoidal, the SVPWM is applied to the voltage inverter. These control methods are based on the current, voltage and torque in the rotating reference frame.

The system equation is Equation (4). The system equation of the coreless BLDCM is transformed by the Clarke and Park transformation and per unit conversion, and decouples the dependent terms using the vector control theorem. The load is a color wheel with inertia. Also, in order to apply the LQR, the integral terms are added to the system equation for the purpose of improving the command following characteristics of the rotating speed.

$$\begin{aligned}\dot{x}_n&=A_nx_n+B_nu_\varepsilon\\ y_n&=C_nx_n\end{aligned} \tag{4}$$

where, $x_n = \begin{bmatrix} x \\ q \end{bmatrix}$, $u_\varepsilon = \begin{bmatrix} i_{dnref} - i_{dn} \\ i_{qnref} - i_{qn} \\ \omega_{rnref} - \omega_{rn} \end{bmatrix}$

$$A_n = \begin{bmatrix} A & B \\ 0 & I \end{bmatrix}, \quad B_n = \begin{bmatrix} B \\ I \end{bmatrix}, \quad C_n = [C \quad 0],$$

$$x = \begin{bmatrix} i_{dn} \\ i_{qn} \\ \omega_{rn} \end{bmatrix}, A = \begin{bmatrix} -R_n / L_n & 0 & 0 \\ 0 & -R_n / L_n & 0 \\ 0 & k_n & 0 \end{bmatrix},$$

$$B = \frac{1}{L_n} I, \quad C = I,$$

$I = 3 \times 3$ unit matrix,

q : integral output of error : $\dot{q} = u_\varepsilon$

u_ε : state variable(i_{dn}, i_{qn}, ω_{rn}) error

i_{dnref}, i_{qnref} : per unit d-axis and q-axis current reference,

i_{dn}, i_{qn} : per unit d-axis and q-axis current,

ω_{rnref} : per unit rotating speed reference,

ω_{rn} : per unit rotating speed,

R_n : per unit phase resistance,

L_n : per unit phase inductance

k_n : per unit torque constant,

The performance index of the LQR is Equation (5), its solution is Equation (6).

$$P = \int [x_n^T Q x_n + u_\varepsilon^T R u_\varepsilon] dt \tag{5}$$

where, $P = x_n^T x_n$: performance index,

Q : positive semi-definite weight matrix,

R : positive definite weight matrix

$$\begin{aligned} & PA_n + A_n^T P + Q - PB_n R^{-1} B_n^T P = 0 \\ & K = R^{-1} B_n^T P \\ & u_\varepsilon = -K x_n \end{aligned} \tag{6}$$

where, $K : 6 \times 6$ gain matrix

From Equation (6), PI controllers for d-axis and q-axis current, and rotating speed are obtained by means of applying gain K. Equation (7) is the PI controller.

$$\begin{bmatrix} v_{dn} \\ v_{qn} \\ i_{qn} \end{bmatrix} = \begin{bmatrix} k_{pd} e_{id} + \int k_{id} e_{id} dt \\ k_{pq} e_{iq} + \int k_{iq} e_{iq} dt \\ k_{p\omega} e_\omega + \int k_{i\omega} e_\omega dt \end{bmatrix} \tag{7}$$

where, v_{dn}, v_{qn} : per unit input voltage

k_{pd}, k_{pq}, $k_{p\omega}$: proportional gain,

k_{id}, k_{iq}, $k_{i\omega}$: integral gain,

$e_{id} = i_{dnref} - i_{dn}$, $e_{iq} = i_{qnref} - i_{qn}$, $e_\omega = \omega_{rnref} - \omega_{rn}$

The voltage components of Equation (7) are added $-\omega_{rn} i_{qn}$, $\omega_{rn} i_{dn} + k_{\omega n} \omega_{rn} / L_{sn}$, respectively and are used to find the DC link voltage reference such as in Equation (8).

The buck converter makes the DC link voltage track it, and the coreless BLDCM rotates it at a constant speed.

$$V_{dcref} = \sqrt{v_{dref}^2 + v_{qref}^2} \tag{8}$$

where, V_{dcref} : DC link reference voltage.

v_{dref} : d-axis voltage reference,

v_{qref} : q-axis voltage reference

5. Finite element analysis of the coreless Brushless DC Motor

The structure of a coreless BLDCM is shown in Fig. 2. The coreless BLDCM is composed of three parts, the ADB, the magnetic bearing, and the electro-magnetic (EM) part. The ADB only has a radial directional load capacity, but does not have the axial directional load capacity. So, the rotor of the coreless BLDCM can be flown up or down because of the rotor and load weight. The magnetic bearing does not have radial directional force but axial directional magnetic force which prevents the rotor from flying.

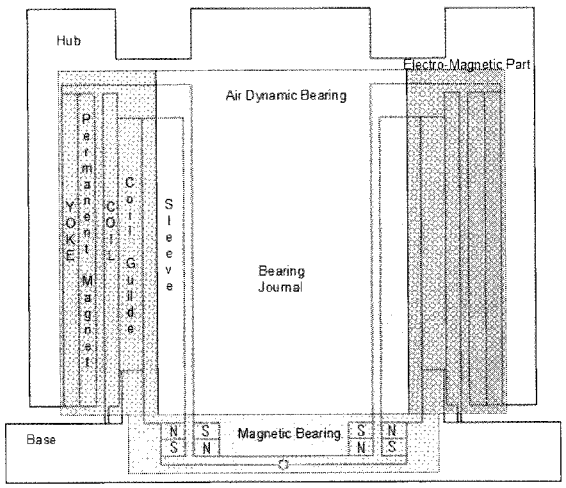

Fig. 2. Structure of coreless BLDCM

5.1 Finite element analysis of an air dynamic bearing

An ADB consists of the bearing journal and sleeve without supports which connects with the body of the rotation and the stator including the coils and the coil guide, respectively. Air is pumped into the bearing clearance between the journal and the sleeve. The rotor is supported by air pressure created when the journal rotates.

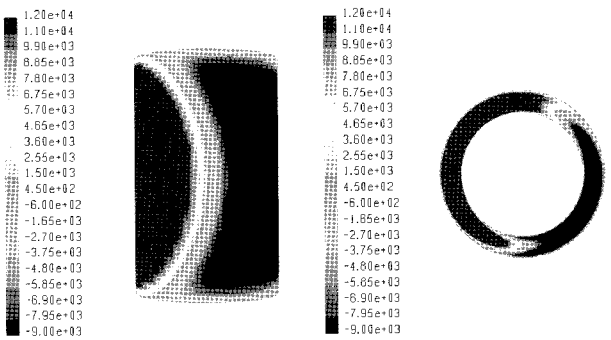

Fig. 3. Air pressure distribution at an eccentricity rate of 0.1

Fig. 3 shows the FEA result for air pressure in the clearance at an eccentricity rate of 0.1 at a rotating speed of 14,400rpm. The air pressure is $1.2x10^4$ N/m^2 in the small gap and $-9x10^3$ N/m^2 in the large gap. The load capacity integrated to the surface is 0.1kg. Fig. 4 shows the FEA result for air pressure at an eccentricity rate of 0.4 at the same speed. The high and low pressure regions are enlarged, and the load capacity is increased to 0.38kg.

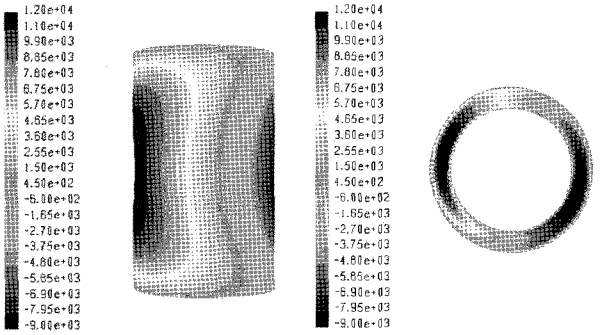

Fig. 4. Air pressure distribution at an eccentricity rate of 0.4

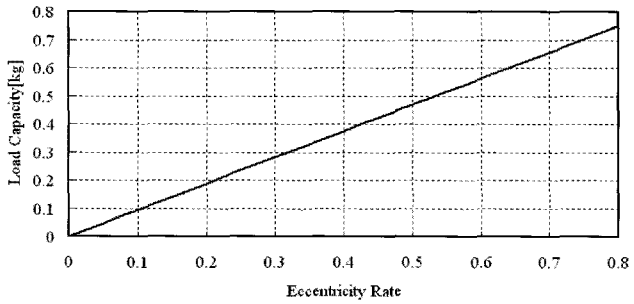

Fig. 5. Load capacity for the eccentricity variation

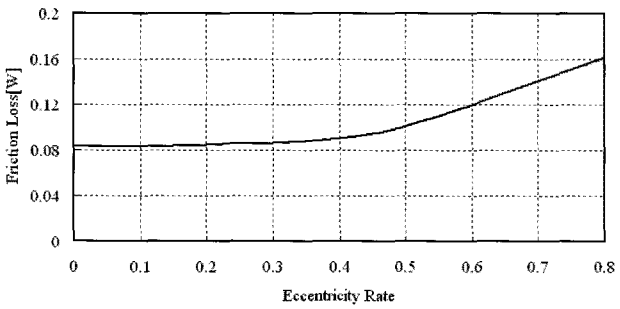

Fig. 6. Friction loss for the eccentricity variation

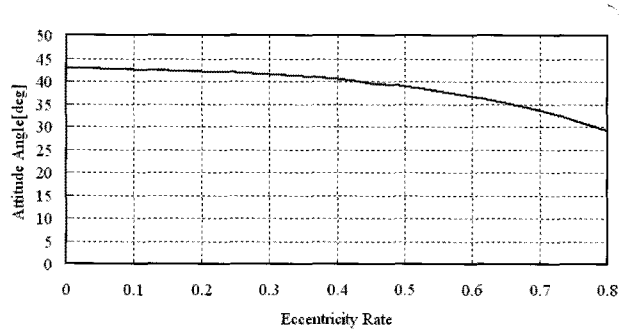

Fig. 7. Attitude angle for eccentricity variation.

Figs. 5 and 6 show the load capacity and the friction loss for the eccentricity variation, respectively. If the eccentricity is bigger, load capacity and friction loss are bigger. Fig. 7 shows the attitude angle for the eccentricity variation. Under an eccentricity of 0.4, the attitude angle is not changed and is 43°. Therefore, the journal of ADB supports the rotor weight and load stably under an eccentricity of 0.4 and has low friction loss and little mechanical vibration. However, with an eccentricity over 0.4, load capacity and friction loss increase and the attitude angle decreases abruptly. The bearing journal doesn't disperse the load and support directly. Consequently, the bearing is unstable and experiences mechanical vibration and mechanical noise due to air friction.

The designed and analyzed coreless BLDCM is stable under an eccentricity of 0.4.

5.2 Electro-magnetic part of a coreless BLDCM

The EM part of a coreless BLDCM consists of the stator and the rotor. The stator consists only of coils and the rotor has a permanent magnet and a rotor yoke. Air acts on the stator yoke which is the flux path of the permanent magnet.

Fig. 8 shows the flux lines of an outer rotor type coreless BLDCM by the FEA. The magnetization waveform of the permanent magnet is sinusoidal and the airgap flux density is 0.22[T]. Although the coils are displaced in the inside of the permanent magnet, the waveform and the value of the flux density are not changed because there is no stator yoke. Fig. 9 shows the line-to-line back EMF waveform of the coreless BLDCM sinusoidal and the back EMF constant is 0.00358Vs/rad.

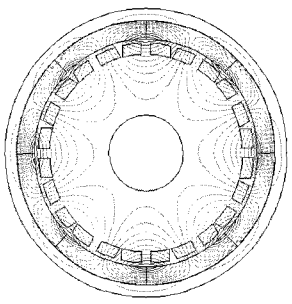

Fig. 8. Flux lines of a coreless BLDCM

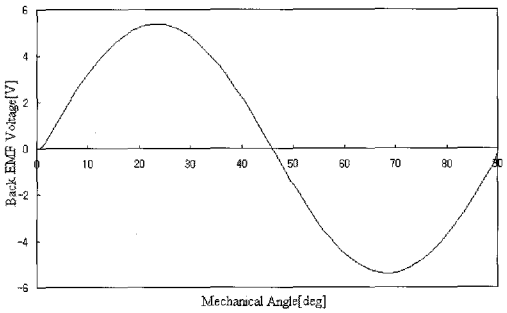

Fig. 9. Line-to-line back EMF waveform of a coreless BLDCM

In order to inspect the effect of the airgap variation, the FEA of a coreless BLDCM is performed assuming that the coils are displaced as 100μm to the upper direction of the airgap by the fabrication error.

Fig. 10 shows the flux lines of the coreless BLDCM at the displacement of the coils as 100μm to the upper direction of the airgap. The flux density in the airgap is the same as the flux density at the no displacement, although the flux of the upper part which came into contact with the coils is different to that of the under part: the former is 0.223T and the latter is 0.212T. Consequently, the unbalanced magnetic force is 2.4g at a rotating speed of 14,400rpm and a phase current of 200mA occurs, as well as an unbalance torque of 0.185gfcm with the same conditions. These are very small. A coreless BLDCM has little the unbalanced force and torque.

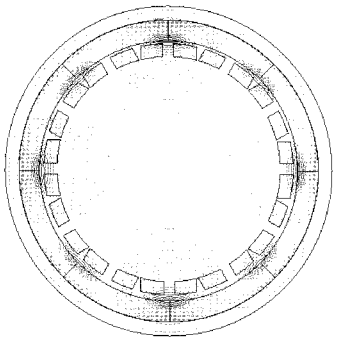

Fig. 10. Flux lines of a coreless BLDCM at an airgap variation of 100μm

5.3 Unbalanced magnetic force of a slotless BLDCM to the air-gap variation

The stator of a slotless BLDCM has coils and a stator yoke which creates the unbalanced force and load torque by fabrication error. If the stator is displaced, the flux between the permanent magnet and the stator at the small airgap part is bigger than at the large airgap part. Therefore, the unbalanced force and the unbalanced torque occur as a result of the flux difference.

In order to investigate unbalanced force and torque, the FEA of a slotless BLDCM is performed assuming that the stator yoke is displaced as 100μm to the upper direction of the airgap by a fabrication error. In Fig. 11, the flux density of the upper part is 0.41T and that of the under part is 0.19T. The unbalanced force is 0.75kg and the load torque is 5.2gfcm. The former causes an ADB to become an eccentric rotation with an eccentricity rate of 0.8, and the latter causes slotless BLDCMs to increase to an input current 145mA. Fig. 12 shows the unbalanced magnetic force to the airgap variation. An airgap variation over 110μm by fabrication error causes an unbalanced force over 0.8kg. The sleeve and journal of the ADB is contacted and destroyed as the maximum load capacity of the ADB is about 0.78kg. An airgap variation over 50μm causes the ADB to vibrate because of its small attitude angle of 40° or under.

Fig. 13 shows the load torque of the airgap variation. As with the unbalanced force, the load torque is very high. No load current is over 200mA with an airgap variation over 110μm.

As a result, a slotless BLDCM with an airgap variation over 100μm is not adequate for a motor using an ADB.

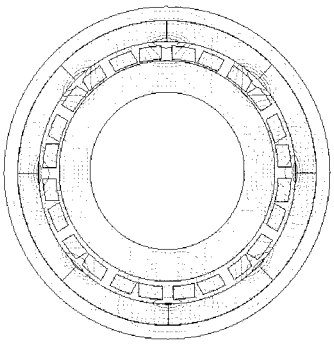

Fig. 11. Flux lines of a slotless BLDCM at an airgap variation of 100μm

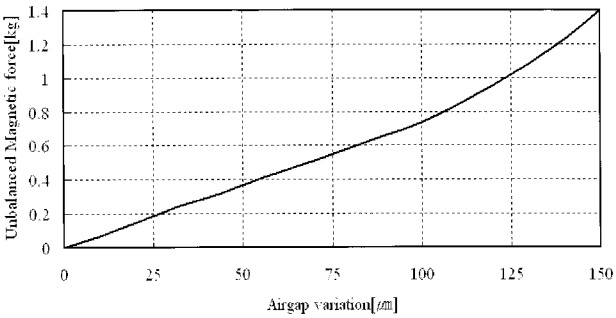

Fig. 12. Unbalanced Magnetic force of a slotless BLDCM to airgap variation

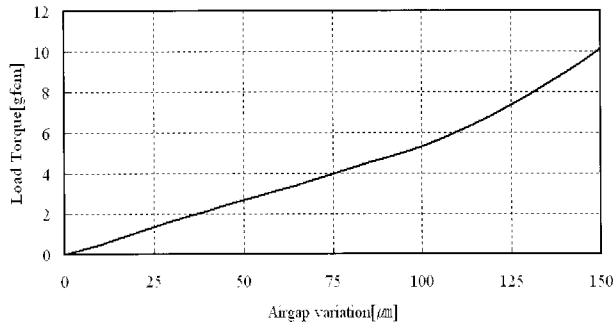

Fig. 13. Load torque of a slotless BLDCM to airgap variation

5.4 Magnetic bearing

The axial directional force of the magnetic bearing makes the ADB stable for up and down disturbances.

Fig. 14 shows the flux direction and flux density of a magnetic bearing using a 3-D FEA when the inner N and S permanent magnet is displaced 200μm from the bottom. The axial directional magnetic force between the inner and outer permanent magnet is -0.32kg and the radial directional magnetic force is 0.0002kg. Although a load of

0.32kg presses the inner permanent magnet, it would not go down 200μm or more. Also, the other parts of the coreless BLDCM are not affected by the magnetic bearing because the radial directional magnetic force is 0.0002kg.

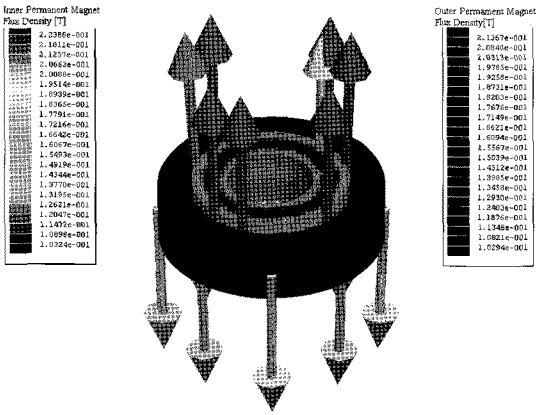

Fig.14. Flux density of a magnetic bearing when the inner magnet is at a rising height 200μm from the bottom

6. Experimental Results

In order to prove the analysis and design of a coreless BLDCM using an ADB, prototype coreless and slotless motors were fabricated and tested. Mechanical vibration, namely the repeatable runout (RRO) and acoustic noise, are measured to inspect the mechanical characteristics of the prototype motors, and phase current, high frequency acoustic noise, and speed error are measured to investigate their electrical characteristics. Also, 120° and 180° conduction type inverters are used to drive them. The former is controlled by a lead angle controller and makes the phase current rectangular, and the latter is controlled by an SVPWM method and DC link controller and makes the phase current trapezoidal. The DC link controller regulates the buck converter to make the DC link voltage tracks the reference voltage which is set by an LQR speed controller.

Table 1 shows the specifications of the prototype coreless motor and the motor drive inverter.

Table 1. Prototype coreless motor and motor drive inverter specifications

Coreless BLDCM		Inverter	
Items	Spec.	Items	Spec'
Poles	4	Input Voltage	12V
EMF const.	0.0035Vs/rad	Input Current	1A
Current Rate	0.15 A	SW Freq.	50kHz
Voltage Rate	12V	Control	120^{o} ,180^{o}

Fig. 15 (a) shows the test equipment used to measure the RRO at the side of the prototype motor hub. Fig. 15 (b) shows the test equipment used to measure acoustic noise at anechoicroom. They have the fixing jig of the prototype motor and an insulating table blocking external noise and electromagnetic waves. A photo sensor is used to measure the distance from the hub to the sensor, and a Dynamic Signal Analyzer (DSA) processes the photo sensor signal and finds the RRO or acoustic noise of the prototype motor. An oscilloscope measures the phase current.

The back EMF voltage is measured to check the electrical characteristics of the prototype coreless BLDCM.

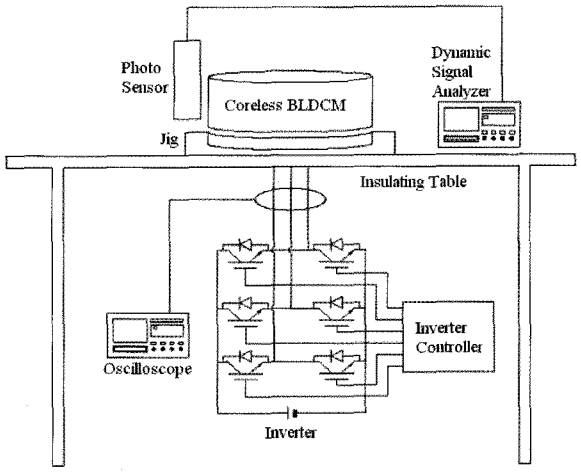

(a) Mechanical vibration measurement

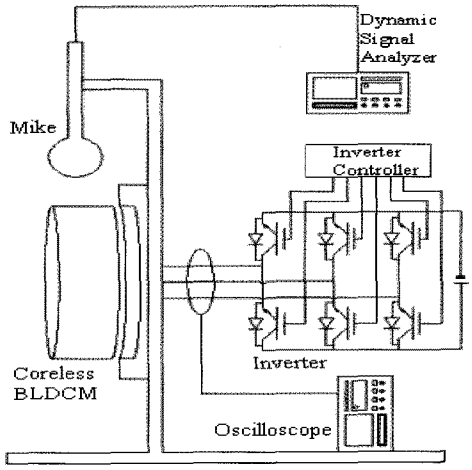

(b) Acoustic noise measurement

Fig. 15. Measurement equipment

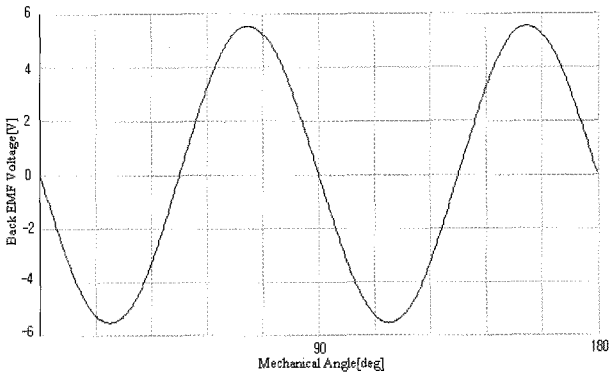

Fig. 16. Back EMF voltage of the prototype coreless BLDCM at a rotating speed of 14,400rpm

Fig. 16 shows the line-to-line back EMF voltage of the prototype motor at a rotating speed of 14,400rpm and the back EMF constant is 0.003515Vs/rad. It is sinusoidal and its peak value is 5.3V. The phase resistance and the inductance of the prototype motor are 4.4Ω and 35μH, respectively. Fig. 17 shows the no load characteristics of a coreless BLDCM driven by a 120° conduction type inverter. The rotating speed in Fig. 17 (a) is 14,400rpm and the rotating speed error between the reference speed and the real speed is 1.4rpm, 0.1% of the reference speed. The precise speed control is accomplished by the lead angle controller.

The phase current in Fig. 17 (b) is 28.3mA, and the estimated input torque is 0.99gfcm, which is composed of 0.437gfcm by a rotor inertia of 5.8gfcm^2 and 0.553gfcm by the ADB's eccentricity. Actually, the RRO in Fig. 17 (c) is 0.9μm, and the eccentricity of the ADB is 0.25. It is similar to the FEA result of the ADB and the coreless BLDCM. The Acoustic noise in Fig. 17 (d) is 26.5dB. The acoustic noise at the mechanical rotational frequency of 240Hz is 19.8dB and is caused by friction between the air and the bearing journal of the ADB at a rotating speed of 14,400rpm. The acoustic noise at a switching frequency of 5.76kHz is 15dB and was created by the peak components of the phase currents caused by the very low electrical time constant $7.96x10^{-6}$ during the commutation period. The phase currents need to reduce the peak current components in order to improve the acoustic noise characteristics.

Fig. 18 shows the no load characteristics of a coreless BLDCM driven by a 180° conduction type inverter. The other characteristics, except acoustic noise, are similar to the characteristics of a coreless BLDCM driven by a 120° conduction type inverter. The rotating speed error in Fig. 18 (a) is 0.9rpm and the phase current in Fig.18 (b) and the RRO in Fig.18 (c) are 28.5mA and 0.95μm, respectively. The acoustic noise in Fig. 18 (d) is 24.9dB. It improved by about 1.6dB more than the acoustic noise of a coreless BLDCM driven by a 120° conduction type inverter because the acoustic noise at high frequency is reduced. The acoustic noise at a mechanical rotating frequency of 240Hz is 19.9dB, which is similar, and the acoustic noise at a switching frequency of 5.76kHz is 10dB, which improved by up to 5dB more than the 15dB shown in Fig. 18 (d). The peak component of the phase currents was reduced by making the phase current waveform trapezoidal, and the acoustic noise at the switching frequency is reduced.

Fig. 19 shows the load characteristics of a coreless BLDCM driven by a 120° conduction type inverter. The rotating speed in Fig.19 (a) is 14,400rpm and the rotating speed error between the reference speed and the real speed is 1.3rpm. The phase current in Fig. 19 (b) is 89mA, and the estimated input torque is 3.115gfcm, which is composed of 2.55gfcm by the rotor inertia of 33.8gfcm^2 and 0.565gfcm by the ADB's eccentricity. Actually, the estimated RRO is 1.05μm and the estimated eccentricity of the ADB is 0.3. However, the measurement RRO in Fig. 19 (c) is 2.1μm because the color wheel surface in the measurement area is not flat. The acoustic noise in Fig. 19 (d) is 52.8dB. The acoustic noise at a mechanical rotational frequency of 240Hz is 39dB caused by the friction between air and the bearing journal of the ADB at a rotating speed of 14,400rpm and the friction between the surface of the color wheel and air. But the wind acoustic noise of the 7-segment color wheel appears at the broad frequency band because it has acoustic noise from the mechanical rotation of the color wheel, by each segment, and by the resonance between every segment, etc. Its frequency band is from 1.68kHz to 11.96kHz because the 7-segments of the color wheel are different in size and shape. Consequently, the electrical acoustic noise is revealed at 11.52kHz, twice that of the switching frequency and at 17.28kHz, three times that of the switching frequency. The electrical acoustic noise at 11.52kHz is 23dB and at 17.28kHz is 19dB. Fig. 20 shows the load characteristics of a coreless BLDCM driven by an 180° conduction type inverter. The other characteristics, except acoustic noise, are similar to the characteristics of a coreless BLDCM driven by a 120° conduction type inverter. The rotating speed error in Fig. 20 (a) and the phase current in Fig. 20 (b) is 0.8rpm and 88.7mA, respectively. The RRO in Fig. 20 (c) is 2.1μm which are the same value as the RRO value of a coreless BLDCM driven by a 120° conduction type inverter. However, the acoustic noise in Fig. 20 (c) is different. The electrical acoustic noise at 11.52kHz is 16dB and at 17.28kHz is 8dB. The improvement effect is up to 7dB. The peak component of the phase currents was reduced by making the phase current waveform trapezoidal. Consequently, the acoustic noise at the switching frequency is reduced.

Fig. 21 shows the no load characteristics of the prototype slotless BLDCM driven by a 120° conduction type inverter at a rotating speed of 14,400rpm. The speed error in Fig. 21 (a) is 1.2rpm and the speed control is precise. The phase current in Fig. 21 (b) is 160mA. It is over 130mA against the phase current of a coreless BLDCM, and the estimated input torque is 5.6gfcm, which is composed of 0.437gfcm from the rotor inertia and 5.163gfcm from the ADB's eccentricity. As a result of the FEA of the slotless BLDCM for the fabrication error, when the ADB's eccentricity rate is 0.83, the unbalanced magnetic force is 0.74kg and the load torque is 5.163gfcm. Actually, the RRO in Fig. 21 (c) is 3.05μm and the ADB's eccentricity rate is 0.86.

It is similar to the FEA result of the ADB and the slotless BLDCM at the fabrication error. Therefore, a slotless BLDCM using an ADB is prone to the fabrication error.

The acoustic noise in Fig. 21 (d) is 28.6dB. The acoustic noise at the mechanical rotational frequency of 240Hz is 24dB and is caused by the friction of from the air and the bearing journal of the ADB at a rotating speed 14,400rpm. The mechanical acoustic noise is created by mechanical vibration and the acoustic noise at a switching frequency of 5.76kHz is 19dB and caused by the peak components.

Tables 2 and 3 show the performance comparison of applied methods. A coreless BLDCM and a 180° conduction type inverter reduce power consumption and high frequency acoustic noise.

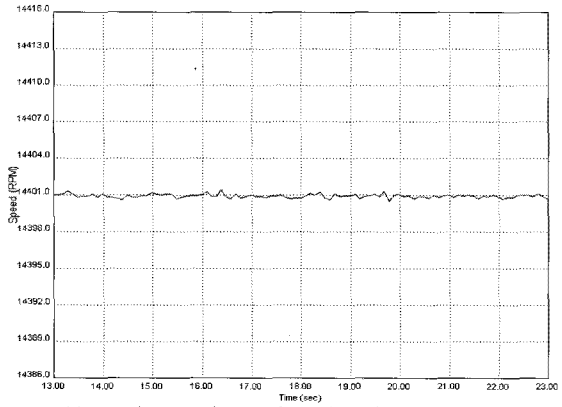

(a) Rotating speed: 14,400rpm (speed error: 1.4rpm)

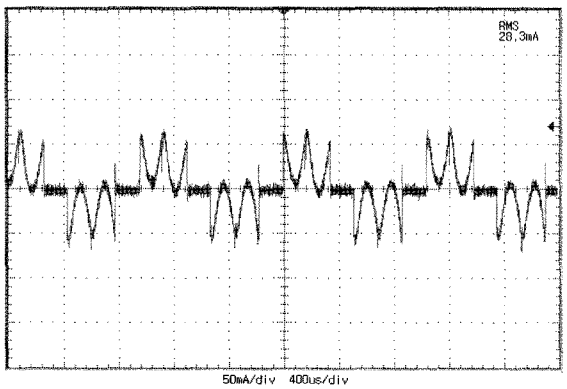

(b) Phase current: RMS 28.3mA

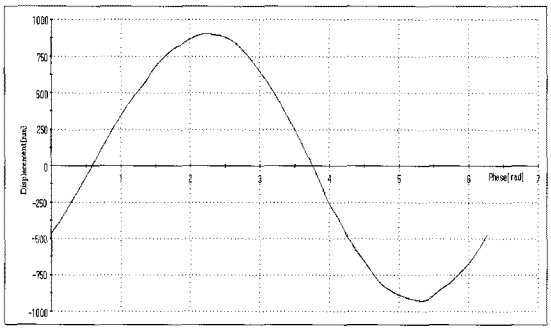

(c) RRO: maximum 0.9μm

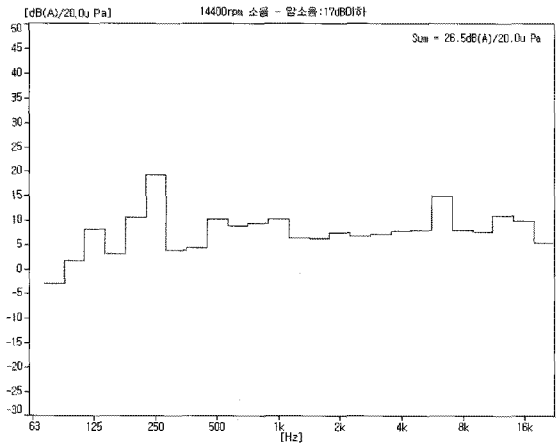

(d) Acoustic noise: sum=26.5dB

Fig. 17. No load characteristics of a coreless BLDCM driven by a 120° conduction type inverter

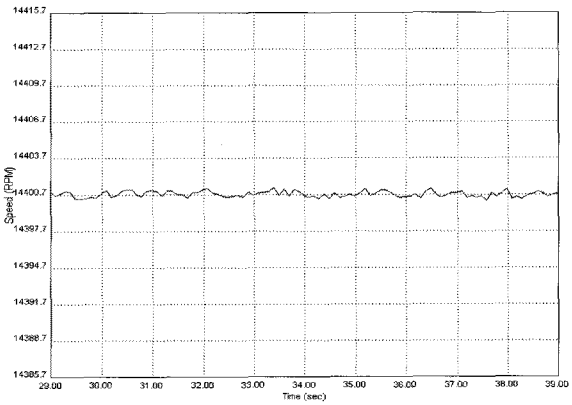

(a) Rotating speed: 14,400rpm (speed error: 0.9rpm)

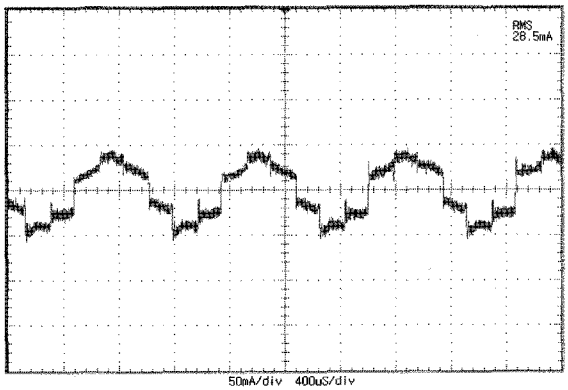

(b) Phase current: RMS 28.5mA

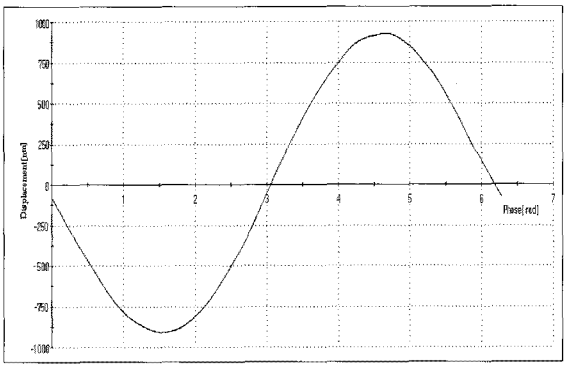

(c) RRO: maximum 0.92μm

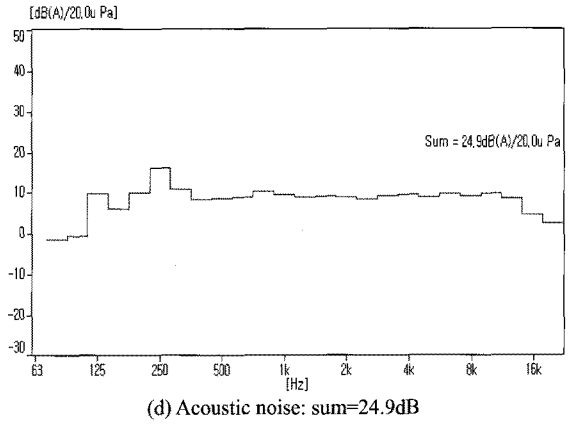

(d) Acoustic noise: sum=24.9dB

Fig. 18. No load characteristics of a coreless BLDCM driven by a 180° conduction type inverter

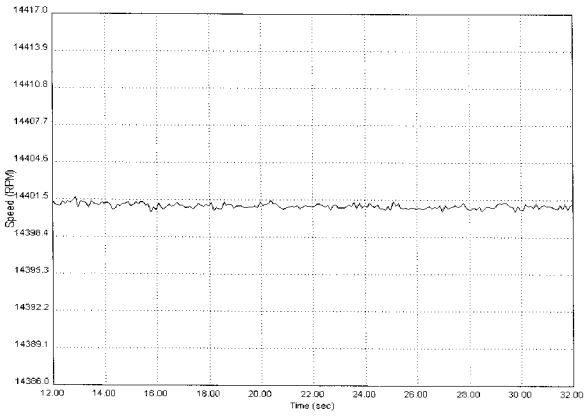

(a) Rotating speed: 14,400rpm (speed error: 1.3rpm)

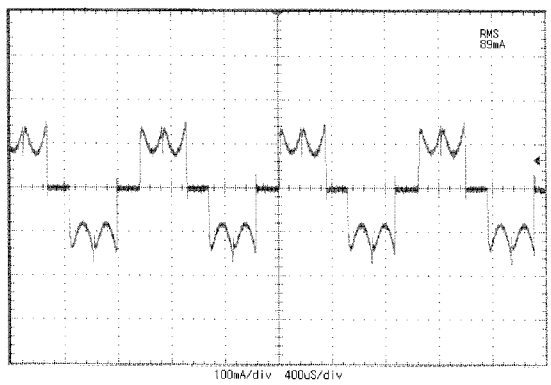

(b) Phase current: RMS 89mA

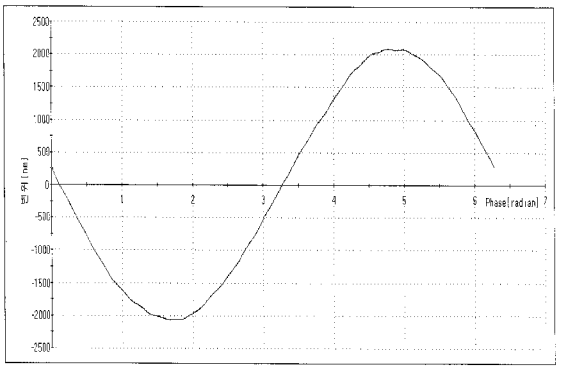

(c) RRO: maximum 2.1μm

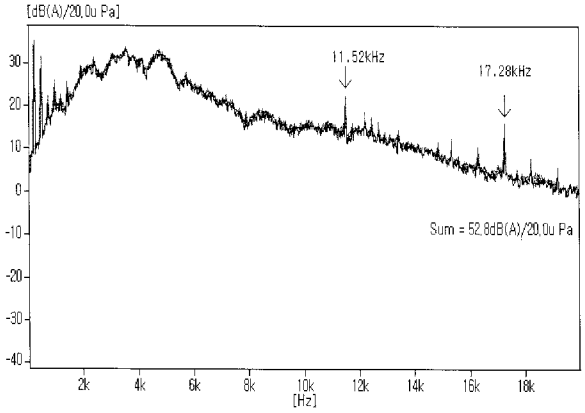

(d) Acoustic noise: sum=52.8dB

Fig. 19. Load characteristics of a coreless BLDCM driven by a 120° conduction type inverter

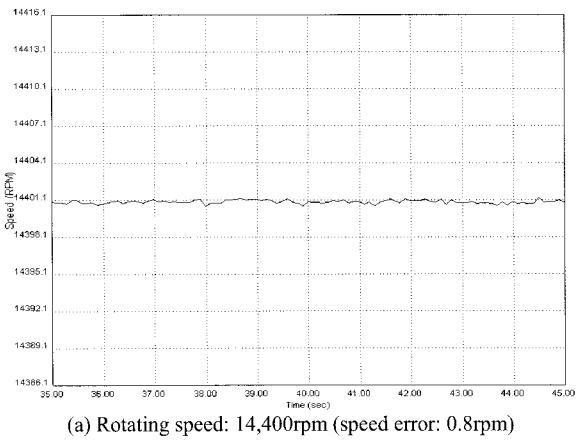

(a) Rotating speed: 14,400rpm (speed error: 0.8rpm)

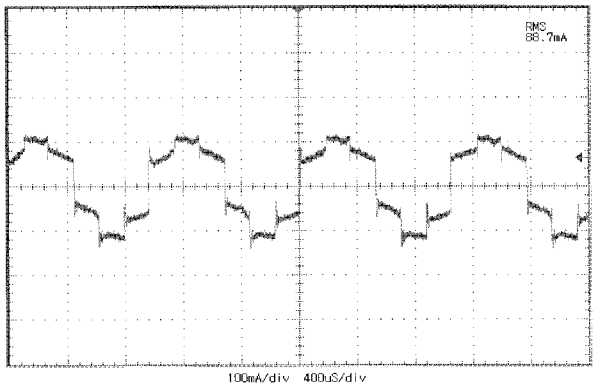

(b) Phase current: RMS 88.7mA

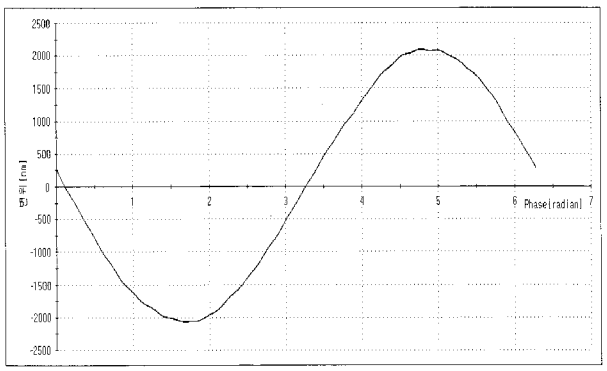

(c) RRO: maximum 2.1μm

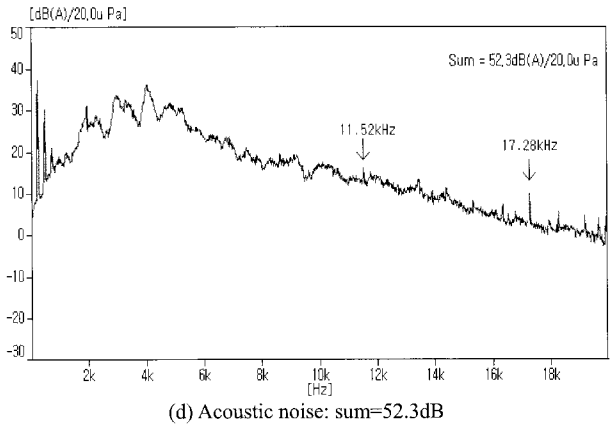

(d) Acoustic noise: sum=52.3dB

Fig. 20. Load characteristics of a coreless BLDCM driven by a 180° conduction type inverter

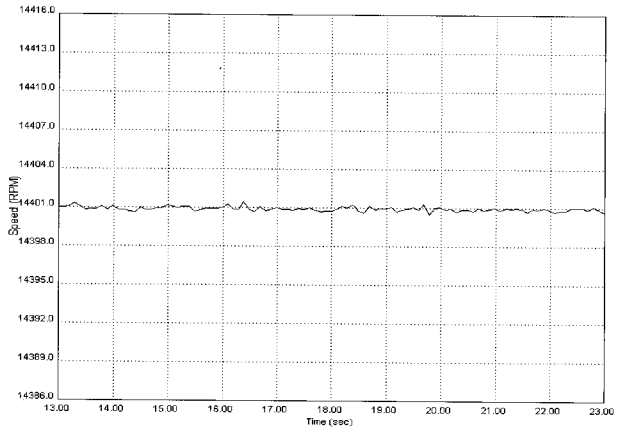

(a) Rotating speed: 14,400rpm (speed error: 1.2rpm)

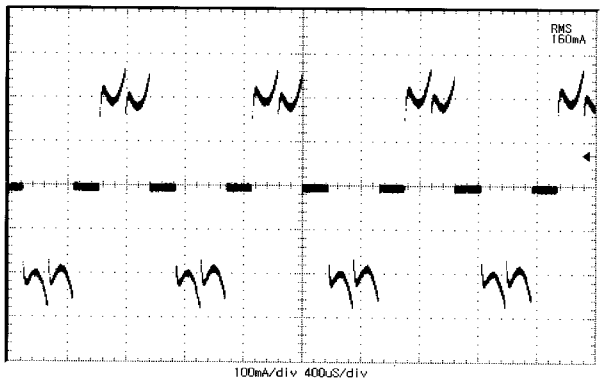

(b) Phase current: RMS 160mA

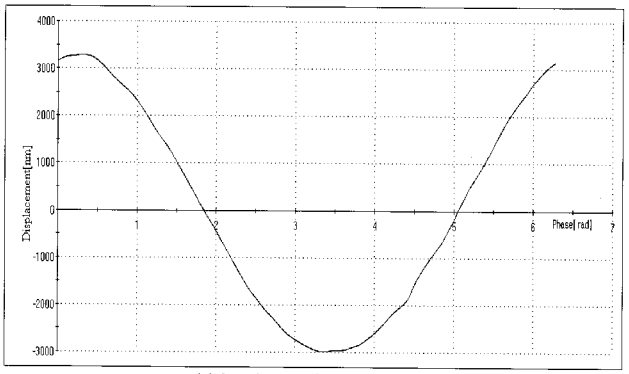

(c) RRO: maximum 3.05μm

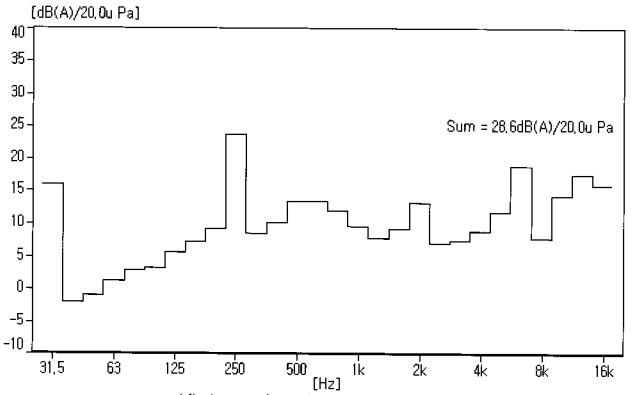

(d) Acoustic noise: sum=28.6dB

Fig. 21. No load characteristics of a slotless BLDCM driven by a 120° conduction type inverter

Table 2. Performance Comparison of a coreless BLDCM with a slotless BLDCM

Items	Coreless BLDCM	Slotless BLDCM
RRO	0.92 μm	2.5 μm
Acoustic Noise	26.5dB	28.6dB
Phase Current	28.3mArms(@9.6V)	160mArms(12V)
Power	0.27W	1.92W

Table 3. Performance Comparison of a coreless BLDCM driven by a 180° conduction type inverter with a 120° conduction type inverter

Items	120° conduction type inverter	180° conduction type inverter
RRO	2.1 μm	2.1 μm
Acoustic Noise	23dB(@11.52kHz)	16dB(@11.52kHz)
Acoustic Noise	19dB(@17.28kHz)	8dB(@17.28kHz)
Phase Current	89mA	88.7mA
DCLink Voltage	10.4V	10.4V
Power	0.93W	0.93W

7. Conclusion

This paper proposes a reduction method of acoustic noise and mechanical vibration for a coreless brushless DC motor with an air dynamic bearing at the fabrication error.

Effects for the fabrication error of a slotless and a coreless brushless DC motor are analyzed using the finite element analysis. The unbalanced magnetic force makes the air dynamic bearing unstable in a slotless brushless DC motor. However, the unbalanced magnetic force of the coreless brushless DC motor is small to the fabrication error. Consequently, mechanical vibration and acoustic noise at the mechanical rotating frequency are small and the phase currents of a coreless brushless DC motor are smaller than those of a slotless brushless DC motor.

The low acoustic noise at a high frequency is achieved by making the phase current trapezoidal. A 180° conduction type inverter drives the coreless brushless DC motor to make the phase current trapezoidal and reduces the peak components of the phase current at the switching frequency. Consequently, the acoustic noises which occurred at a high frequency over the switching frequency are reduced.

Acknowledgements

This work was supported by Inha University.

References

[1] Ackermann, B, Janssen, J.H.H., Sottek, R., and van Steen, R.I., "New technique for reducing cogging torque in a class of brushless DC motors", IEE Proceedings 139, no. 4, 315-320, 1992.

[2] Hendershot Jr., J. R., and Miller, T. J. E., *Design of brushless permanent-magnet Motors*, Magna Physics Publishing and Clarendon Press, 8-1~8-19, 1994.

[3] Jouve, D., and Bui, D., "Torque ripple compensation in DSP-Based brushless servo drive, Intelligent Motion", PCIM Proceedings, Nurnberg 28-37, 1993.

[4] Miller, T.J.E., and Hughes, A., "Comparative design and performance analysis of air-cored and iron-cored synchronous machines", IEE Proceedings 124, 127-32,1997.

[5] Boules, N., "Two-dimensional analysis of cylindrical machines with permanent magnet excitation", IEEE Transactions, vol.I A-20, no. 5, pp. 1267-1277, Sept./ Oct. 1984.

[6] Zhang, Qide, Chen, Shixin, Winoto, S. H., and Ong, Eng-Hong, "Design of high-speed magnetic fluid bearing spindle motor", IEEE Trans. Magn., vol. 37, no. 4, pp. 2647-2650, July 2001.

[7] Hwang, Sang-Moon, Kim, Kyung-Tae, Jeong, Weui-Bong, Jung, Yoong-Ho, and Kang, Beom-Soo, "Comparision of vibration sources between symmetric and asymmetric HDD spindle motors with rotor eccentricity", IEEE Trans. Industry App., vol. 37, no.6, pp. 1727-1731, Nov./Dec. 2001

Iee-Woo Yang received his Ph.D. degree in electrical engineering from Inha University, Korea, in 2008. He has been working in ADT.

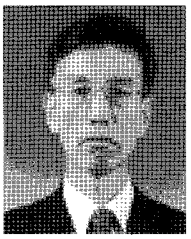

Young-Seok Kim received his B.S. degree in Electrical Engineering from Inha University, Korea, in 1977, and his M.S. and Ph.D. degrees in Electrical Engineering from Nagoya University, Japan in 1984 and 1987, respectively. In 1989, he joined Inha University in Korea where he is currently a Professor in the School of Electrical Engineering. His Current research interests Include sensorless motor drives, active power filters and power converting for renewable energy.

Sang-Uk Kim received his Ph.D. degree in Electrical Engineering from Inha University, Korea, in 1998. He joined Inha Technical College in Korea where he is currently a Professor in the School of Electrical Engineering.